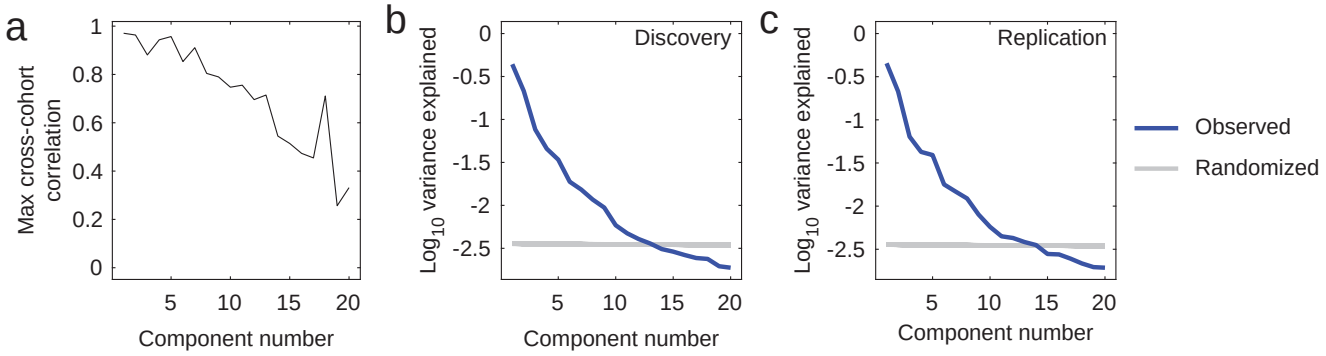

FIG. S1. **Cross-cohort analysis of principal components.** (*a*) For each PC in the discovery dataset (cohort 1), we calculated the maximum correlation with any of the first 20 PCs in the replication dataset (cohort 2).(*b*) Variance explained by the first 20 principal components in the discovery dataset. The blue curve shows observed values while the gray curve shows values expected under a chance model. (*c*) Same plot as panel *b* but for the replication dataset.

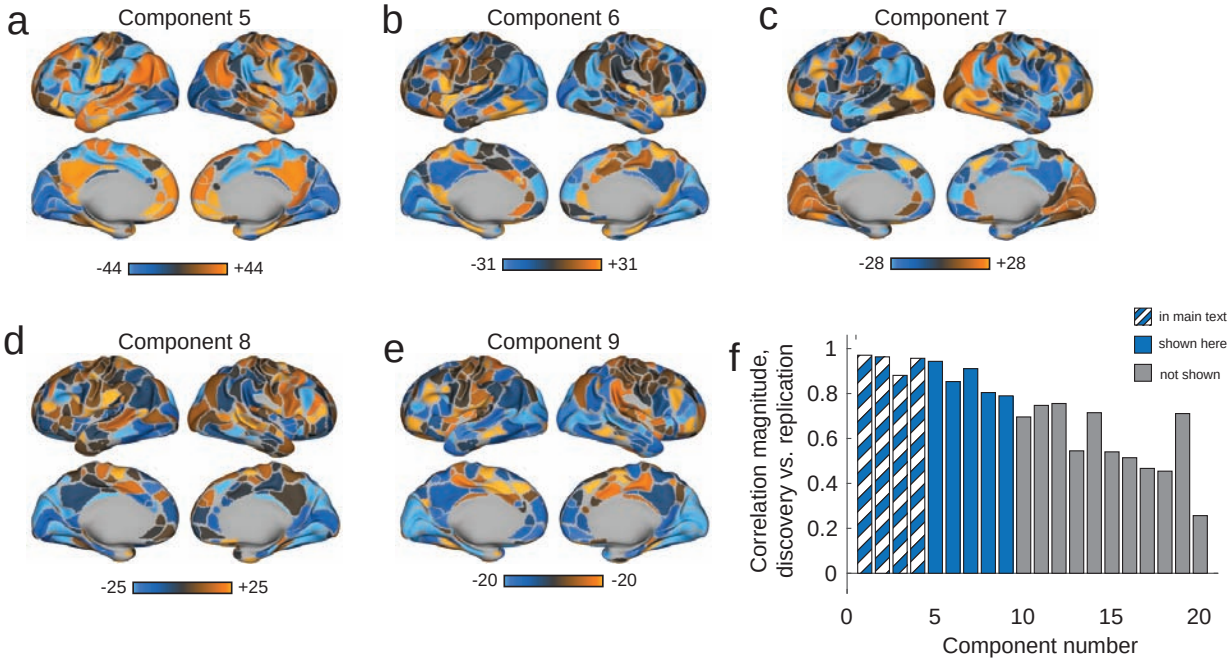

FIG. S2. **Additional components from the HCP dataset.** In the main text we describe a procedure for decomposing intersubject modular variability into principal components and show, as examples, surface projections of those components. Here, we show the next five components (panels *a*-*e*). These components are observed in both the discovery and replication HCP cohorts. We show in panel *f* cross-cohort correlation magnitude, with larger values indicating greater correspondence across cohorts.

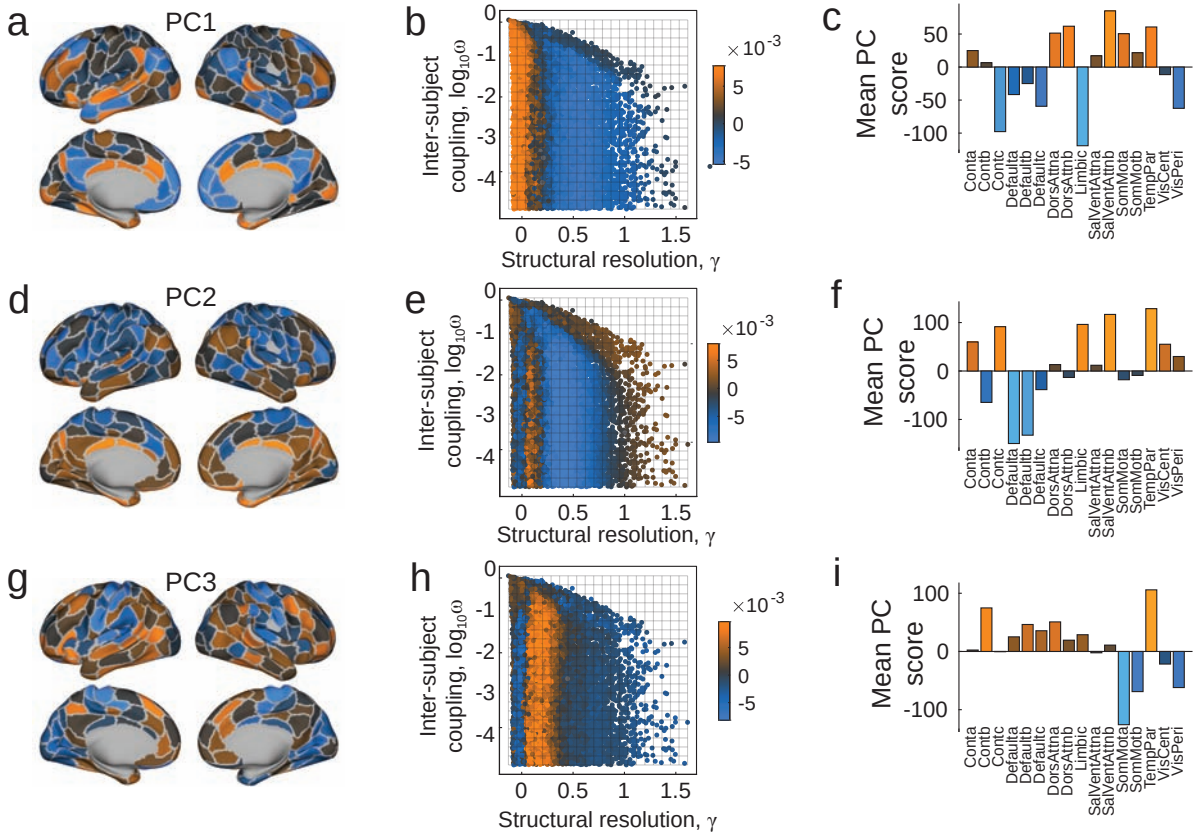

FIG. S3. **Analysis of intersubject community variability using a different parcellation.** These figures are analogous to Fig. 4 in the main text. They depict the spatial scores of the first three principal components (*a*, *d*, *g*), the coefficients of those same components plotted in the $\{\gamma, \omega\}$ parameter space (*b*, *e*, *h*), and the overlap of spatial scores with pre-defined system labels (*c*, *f*, *i*). Although the overlap is inexact, these components bear striking resemblance to those obtained using an alternative parcellation of the brain into $N = 333$ nodes. Notably, when γ is small (*a*-*c*) components of the default mode are invariant across subjects. As γ increases, we find evidence of different modes of variability, including a mode in which visual and motor areas are invariant (*g*-*i*). These patterns are similar to PC1 and PC4 presented in the main text.

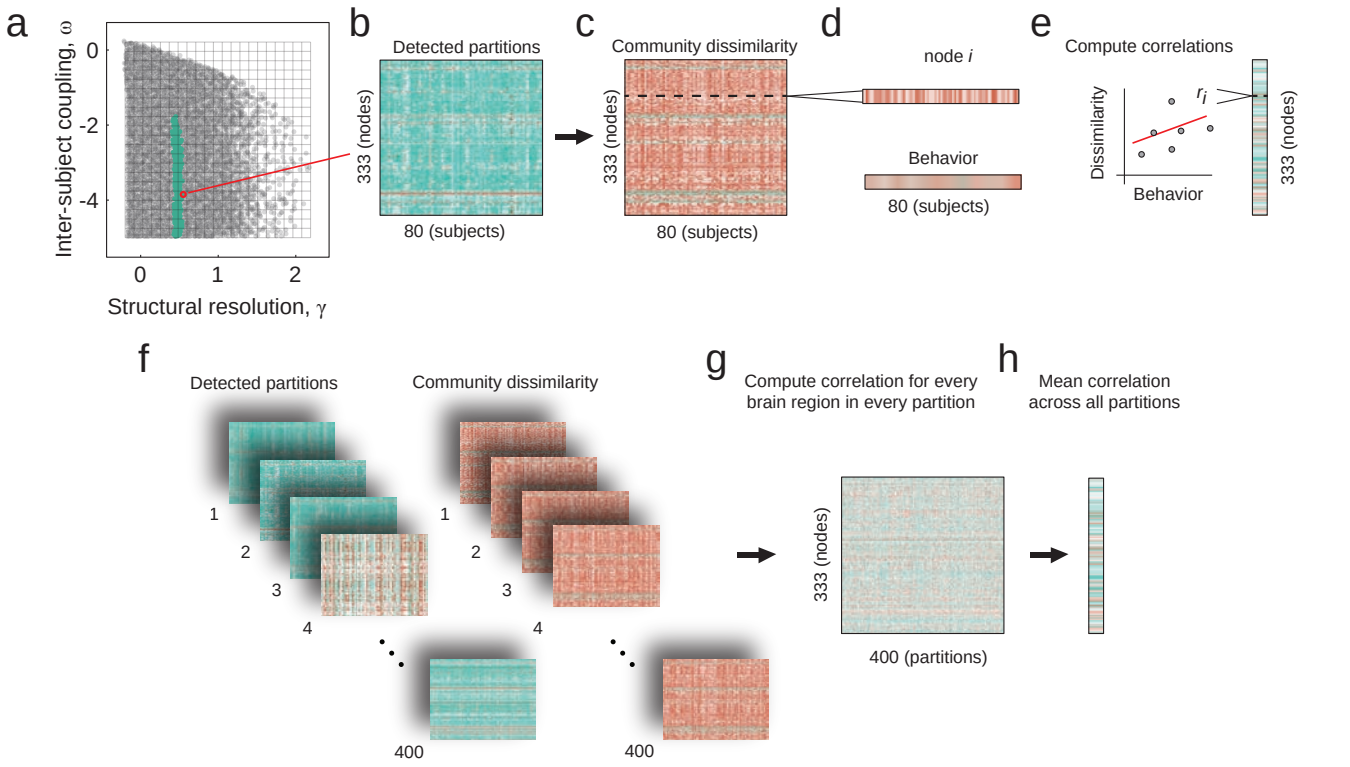

FIG. S4. **Schematic illustrating computation of brain-behavior correlations.** To compute brain-behavior correlations, we identified for each principle component, the 400 partitions with the strongest PC coefficients. We show in panel *a* the set of partitions that correspond to PC3, as an example. (*b*) Each point corresponds to a detected partition, in which each of the 333 nodes in all 80 subjects were assigned to one community. (*c*) For each partition, we calculated a subject- and node-level measurement of dissimilarity. Here, red colors indicate that a node's community assignment in a given subject is, on average, dissimilar across subjects; green colors indicate high levels of similarity across subjects. (*d*) We compute brain-behavior correlations on the basis of these dissimilarity measurements. Specifically, we extract the dissimilarity of node i across subjects and compute its similarity with a behavioral or cognitive performance measure. (*e*) Then we compute their linear correlation (Pearson) and repeat this procedure for each of the 333 nodes. (*f*) We applied this procedure to each of the 400 partitions and their corresponding community dissimilarity matrix. (*g*) This process generated 400 brain-wide correlation patterns, over which we averaged. (*h*) In turn this averaging process generated a single mean correlation pattern. Patterns for each behavioral measure and PC are shown in Fig. 6 and Fig. S5.

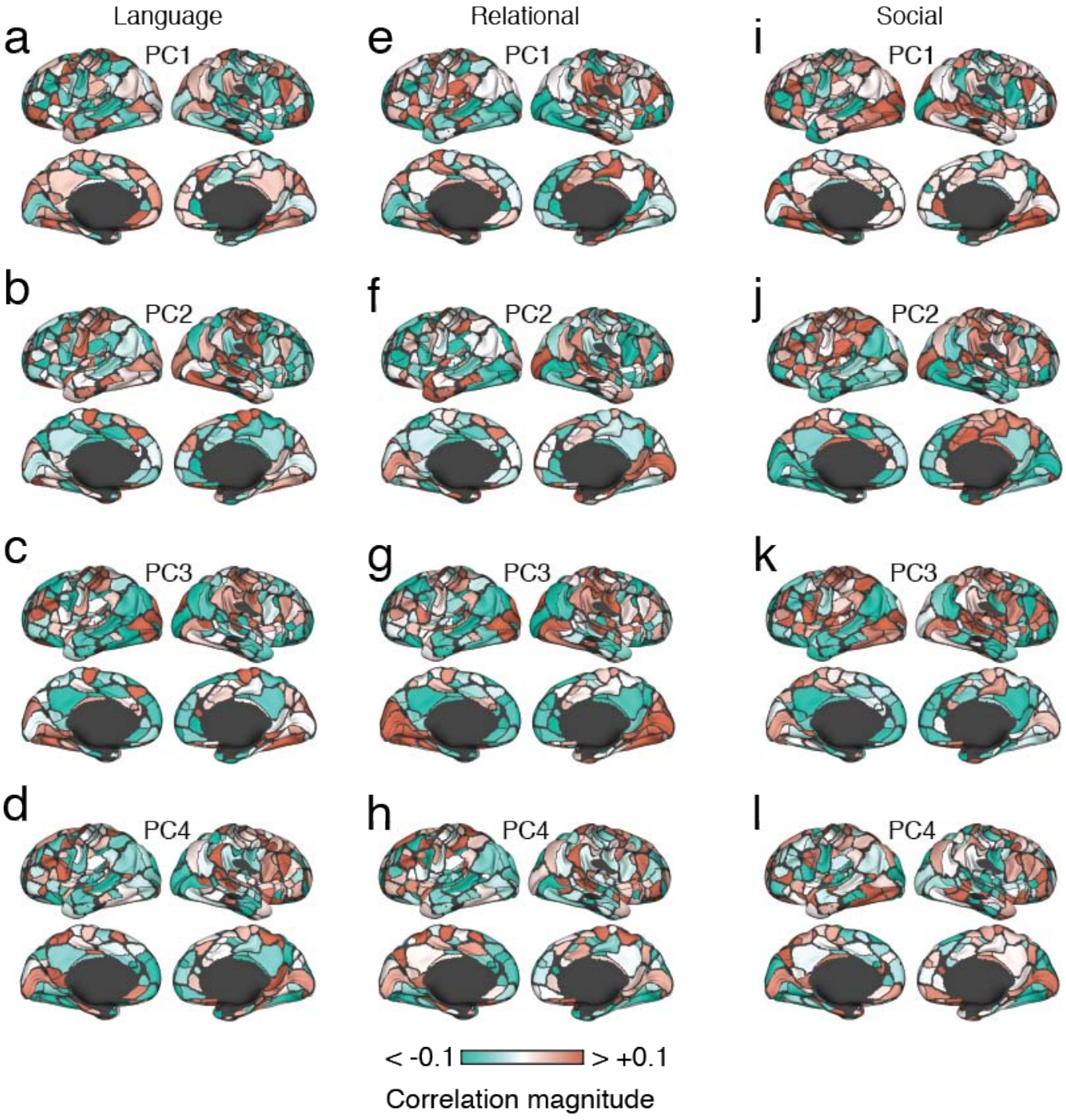

FIG. S5. **Spatial maps depicting the correlation of community structure with measures of task performance.** In the main text we calculated the correlation of community variability with performance on the working memory task and plotted the strength of correlation onto the cortical surface. Here, we show similar surface plots for the Language, Relational, and Social tasks. We also computed correlations separately for the first four modes (principal components) of inter-subject community variability. Each panel in this figure corresponds to the correlation of one behavioral measure for a single principal component.

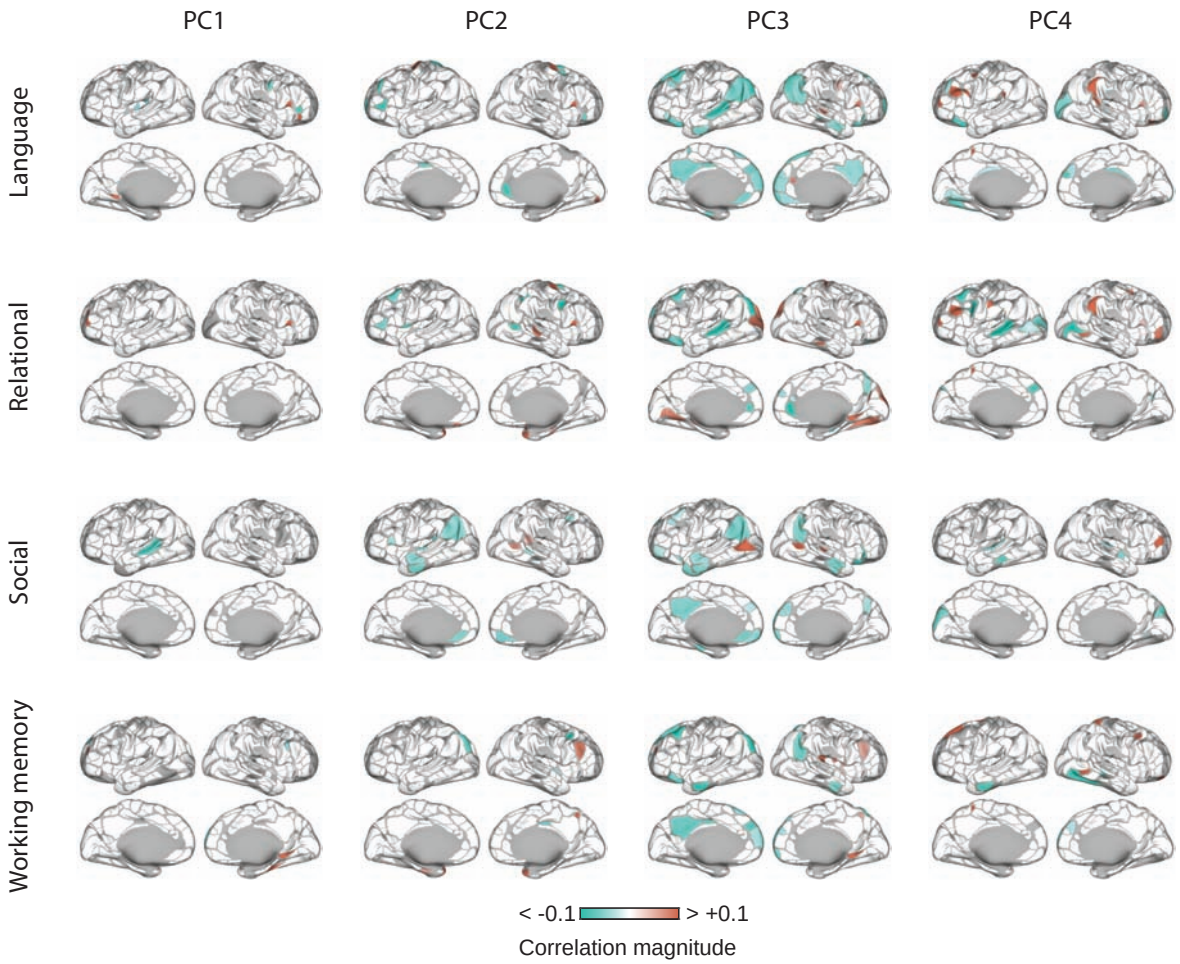

FIG. S6. **Effect of statistical tests on correlation maps.** The average correlation patterns shown in Fig. 6 in the main text are unthresholded. Here, we show identical maps after imposing a two-step process that controls for multiple comparisons. The first step involved correcting for multiple comparisons at the level of single partitions. Specifically, we computed an adjusted critical value given an accepted false discovery rate of $q = 0.05$. This procedure identifies, for a specific partition, the brain areas with statistically significant correlations. However, these areas may vary across partitions. To identify areas that are *consistently* statistically significant across multiple partitions, we computed for each area the fraction of times that its correlation magnitude exceeded the statistical threshold and compared this fraction to the same value computed under a permutation-based null model (100 randomizations) in which we uniformly and randomly permuted node order independently for each partition. We then computed non-parametric p-values and, again, controlled the false discovery rate at $q = 0.05$ to identify brain areas that are *consistently* identified as statistically significant. We repeated this full procedure for each principal component and for each behavioral measure, the results of which are summarized here.

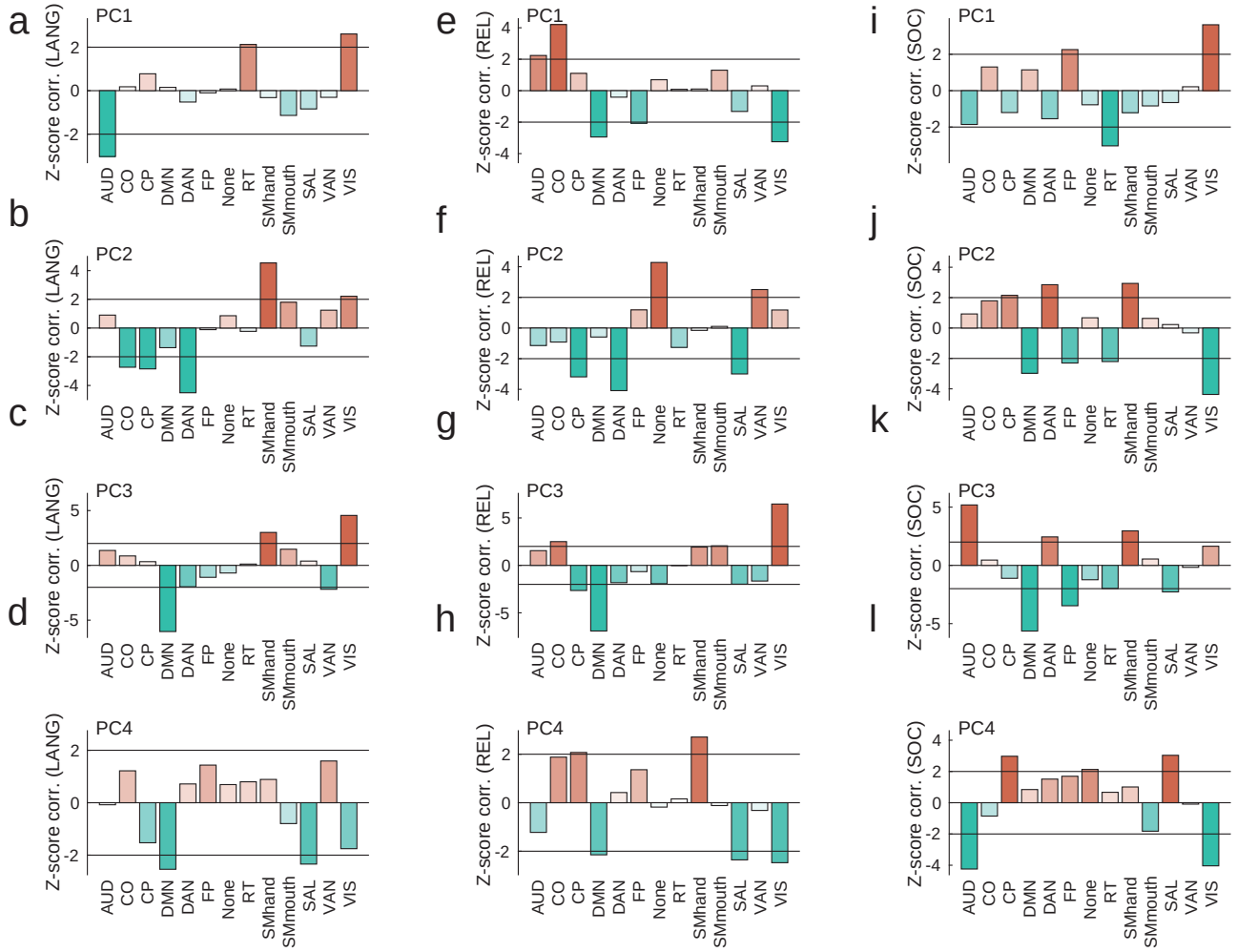

FIG. S7. **System-level maps depicting the correlation of community structure with measures of task performance.** In this figure, we aggregated the regional correlation coefficients by cognitive systems and compared the mean system correlation to what we would expect by chance. Here, we report z-scored correlations. In general, larger positive z-scores indicate stronger than expected system-level correlations.

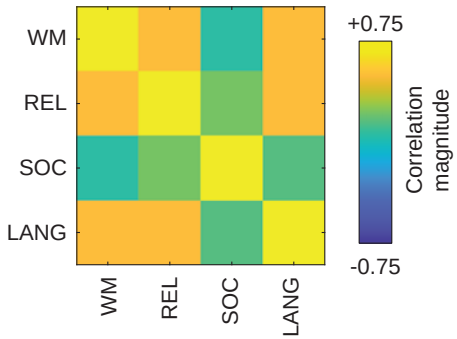

FIG. S8. **Correlation of behavioral measures across subjects.** We calculated pairwise correlations for all behavioral measures. We note that, in general, these measures are correlated with one another. In particular, working memory (WM), relational (REL), and language (LANG) are all strongly correlated with one another.

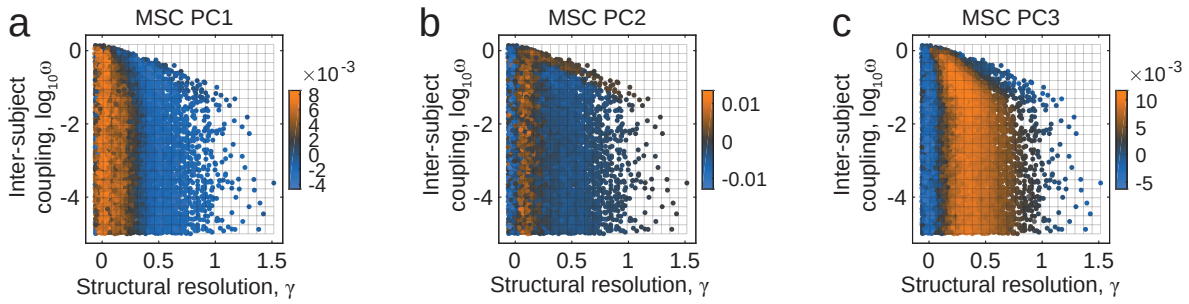

FIG. S9. **Projections of Midnight Scan Club principal components into the $\{\gamma, \omega\}$ parameter space.** This figure is analogous to Fig. 4 in the main text. As in that figure, we find that that the MSC PCs exhibit clear γ-dependence – note the vertically-oriented striations.